

# Optimal Power Management and Control of Hybrid Photovoltaic-Battery for Grid-Connected Doubly-Fed Induction Generator Based Wind Energy Conversion System

Sahar A. Nasef<sup>1, 4</sup>, Amal A. Hassan<sup>1</sup>, Hanaa T. ElMadany<sup>1</sup>, Mohamed B. Zahran<sup>1, 2</sup>, Mohamed K. El-Shaer<sup>3</sup>, Almoataz Y. Abdelaziz<sup>4</sup>

<sup>1</sup> Electronics Research Institute, Cairo, Egypt

<sup>2</sup> National Authority for Remote Sensing and Space Sciences, Cairo, Egypt

<sup>3</sup> Department of Electrical Engineering, Faculty of Engineering, Al Azhar University, Cairo, Egypt

<sup>4</sup> Department of Electrical Power and Machines, Faculty of Engineering, Ain Shams University, Cairo, Egypt

(Sahar\_Nasef@eri.sci.eg, amal.elramly@eri.sci.eg, hanaa\_tolba@eri.sci.eg, mbazahran@eri.sci.eg, MohamedMahmoud51.el@azhar.edu.eg, ayabdelaziz63@gmail.com)

*Received: 27.01.2022 Accepted: 28.02.2022*

**Abstract:** A doubly-fed induction generator (DFIG) is considered one of the most suitable generators for the variable wind speed due to its different composition from the rest of the other generators. This paper presents optimal design, power management, and control of hybrid photovoltaic (PV) and battery energy storage systems (BESS) for grid-connected DFIG Based wind energy conversion systems (WECS). The proposed system integrates the BESS-PV hybrid system with the DFIG grid-connected system via the DC-link of the back-to-back converter. The main objective of the paper is to maintain a constant DC-link voltage (V<sub>dc</sub>), keep the stator and rotor currents stable and smooth, and maintain constant and smooth active power during the variation in wind speed. The proposed optimized control methodology includes a moth-flame optimized fuzzy logic controller (MFO-FLC) to extract the maximum power of PV power under variable solar radiation. Moreover, a constant-current constant-voltage controller (CC-CV) for BESS is implemented using MFO-PI. MATLAB/ SIMULINK® platform was used to verify the design and control of the proposed system. The simulation results demonstrated the effectiveness of the optimized control methodology under variable solar radiation and wind speed conditions. The active power transferred to the grid through the grid side converter of the DC-link is smoothed and maximized by approximately 22% from its actual value during low wind speed and 1000 w/m<sup>2</sup> while preserving a constant DC-link voltage during transient and steady-state conditions.

**Keywords** Doubly-Fed Induction Generator, Wind Energy Conversion System, Photovoltaic, Battery Energy Storage System, Fuzzy Optimal Control, Moth-Flame Optimizer.

## 1. Introduction

A Hybrid Wind-PV system (HWPVS) is a large-scale integrated system that combines two or more renewable energy sources with energy storage devices such as a battery bank, flywheel, supercapacitors, or a fuel cell. HWPVS is becoming more and more popular for power generation applications with the advancement of renewable energy technologies. These systems are attractive because multiple sources can complement each other to provide more reliable electricity to the consumer than a single-source system. To ensure optimization of power supply conditions for local

loads, WECS and PV systems must be compatible with auxiliary energy storage systems [1] [2]. Based on the foregoing, solar and wind energy are among the most reliable sources of renewable energy at present, as wind energy provides a lot of energy for most countries. The global wind energy market was expected to grow even more in 2019, and indeed this has been done with the total installed capacity reaching 597 GW [3] [4]. But due to their intermittent nature, systems based on wind and solar energy are unreliable without the use of energy storage technologies. Since wind and solar energy are complementary to each other, combining both improves the reliability of the energy source

[5]. The literature on the wind-solar hybrid system has been widely discussed and varied. For wind turbines, this interpretation often depends on the options available number of blades, the direction of rotation, the rotor speed is variable or constant, direct generator or gearbox, induction or synchronous generator. Because wind speeds occasionally exceed the rated wind speed, the effective power is typically regulated by the standard stall concept: when the wind speed exceeds the rated wind speed, the power factor restrictions change, but the energy produced by the turbine remains constant. Two variants of this model, variable pole squirrel cage induction generators (SCIG) and a variable speed limited wound rotor induction generators design, have been used to overcome some of those problems. When wind speeds exceed the rated wind speeds, pitch modulation limits the power output of variable speed wind turbine (WT) with brushless generators, motors, and inverters to rated power. Regardless, fully-rated transformers have higher losses and are significantly more expensive than partial-rated transformers such as DFIG. However, in the case of PMSGs and SCIGs, numerous approaches are utilized controller parameters and increase efficiency, this system is available in a range of configurations for both PMSGs and SCIG [6] [7]. In [8] [9] described a novel self-configuring control technique for increasing the efficiency of grid-connected PMSG-based wind turbines while maintaining low computational complexity. As a result of this enhancement, he built an ideal control system based on the Linear-Quadratic Controller, which consists of two similar and inexpensive frequency converters. Additionally, the author proposed a detailed approach that makes use of the innovative Grey Wolf Optimizer and Hybrid Cuckoo Search techniques. The objective was to determine the optimal variables for the PI controllers in the PMSG wind turbine. The technique of Least Mean Square Root Exponential which was naturally normalized using the negative absolute error exponent specified in [10], is based on the negative square root of the absolute error function, this method is self-contained. This strategy was employed in the research to maintain control and to obtain more consistent outcomes and performance. In [11], an ideal scheme for fuzzy logic strategy has been presented and studied to reduce the overall integrated error. Maximum wind energy extraction is optimized and faults are minimized for grid-connected WT. At present, DFIG with adjustable speed WT and power ratings exceeding 1.5 MW is currently the most often utilized machine for commercialized wind power generation [12]. Additionally, to a low-cost DFIG standard and a partially rated converter feeding the rotor winding, DFIG is defined by a multi-stage drivetrain. Besides that, pitch adjustment maintains rated power output when wind speeds exceed rated speeds [12] [13]. The characteristic of DFIG is that the converted power rate is approximately 25% to 30% of the rated power, this rate is sufficient to produce the rated active power as the speed ratio can be maintained at an appropriate level in most of the operating times [14]. When compared with the constant speed system, it is found that DFIG provides a more stable match with mechanical loads, the power quality is better; the audible noise is lower, improving the wind system's efficiency. In some literature, as will be explained, the PV system's output is connected to the DFIG

to achieve a hybrid DFIG system for an autonomous application [15][16]. This hybrid technology is described by a few researchers, but it was not enough to explain the advantages of this system and whether the performance has been improved or not. The strategy defined in [17] [18] is based on a relatively complex control method that makes use of machine parameters and a large number of PI controllers. In [19], an estimation system was proposed in RSC, and an efficient technique was used to track the maximum power of PV. In [20], the authors explained a hybrid autonomous wind-solar system, which is a four-wire distribution network consisting of WECS-DFIG and PV with battery energy storage technology. The control technique is to estimate the position of the rotor along with determining its speed and current, using indirect vector control algorithms. All of the previously investigated various control strategies based on DFIG with or without storage systems for a standalone system. The authors in [21] used PMSG and BESS which were connected to the DFIG rotor via a back-to-back converter. While PMSM is controlled and designed to maintain constant current link voltage under different mechanical speed conditions, battery power management technology was used to mitigate wind power fluctuations. In [22] and [23], to regulate the active power for the autonomous operation of a DFIG-based wind turbine, a hybrid storage system composed of a battery and a supercapacitor is used. The supercapacitor is connected to DFIG's back-to-back DC connection via a bidirectional buck converter, and the battery storage system is connected to the load side of the system to satisfy the constant component of the demand generation mismatch as well as to avoid deeper discharge. In [24] [25], the author proposed a method for compensating for the wind turbine's inertia weakness by coordinating control between the DFIG and the energy storage system, which can provide frequency support. In this context, a study was published to examine the feasibility of using a BESS to provide an inertial response in a system with significant wind energy penetration [26]. In [27], to improve the frequency regulation capacity of a DFIG-and-energy-storage system, a coordinated Fuzzy-based control method is used. The frequency fluctuation is determined by FLC, and the frequency support is coordinated with the storage system connected to the wind farms at the point of common coupling. In [28], a control of DFIG based on MPPT was explained under the usual conditions to keep improving the wind system's efficiency by adding a control loop to the RSC. In [29], a coordinated strategy for a DFIG integrated with BESS to provide frequency management was presented regarding the control of microgrids with a high wind energy penetration. In [30], a system based on DFIG with a PV system is created to overcome the drawback of individual PV and wind energy sources. MPPT technique, DC-link voltage control, active and reactive power, and grid voltage support control are all implemented using the integrated control for GSC and RSC. A microgrid based on DFIG and a PV array interfaced to the grid is presented in [31], The (RSC) control is meant to achieve MPPT from the wind as well as unity power factor at the DFIG stator terminals. This improves MPPT from both wind and solar energy sources while maintaining grid power flow regulation. Despite some literature has achieved regulated power flow in the grid

according to previous references. However, many of them rely on conventional control methods, which reduces efficiency and makes the response to changing wind speed slow compared with intelligent control [25]–[31]. On the other hand, studies that depend on energy storage systems are charged at speeds higher than the specified speed only [24], [26], [28] [29]. The proposed system is characterized by the fact that the batteries are charged using PV rather than wind. As a result, the active power delivered to the grid is maximized at low wind speeds by the proposed PV-BESS system.

This paper presents an optimal design, control, and power management of grid-connected DFIG based WECS using a hybrid PV-BESS system connected to the DFIG through the DC-link of the back-to-back converter. The main contributions of this paper are to provide a new strategic optimal design and control of hybrid wind PV-BESS system. The proposed methodology depends on integrating the PV-BESS system into the DC-link of the back-to-back converter of a DFIG to obtain optimal power management and an excellent behaviour resulting in improved overall system performance under variable solar radiation and wind speed conditions. An OFLC has been done for scaling factors for GRC and RSC controllers by applying the MFO-FLC technique to get the best values.

PV array with a boost DC-DC converter is used in the proposed system and the MFO-FLC method has been

implemented as an MPPT technique to extract maximum power from PV under variable solar radiation conditions. In addition, an optimized constant-current constant-voltage (CC-CV) PI controller for BESS charging and discharging control is carried out using the MFO technique to obtain an optimal performance, which makes the system more stable and gives the best results.

Finally, a comparison will be made between the proposed optimized modified system and the system using a PI controller for RSC and GSC without BESS and PV to clarify that the proposed system is more effective with the best results and the highest efficiency. MATLAB/ SIMULINK® platform was used to implement the modeling and optimized control of the proposed system.

## 2. Configuration and Control Strategy of Proposed System

Figure 1 illustrates the configuration of grid-connected WECS with modified DFIG by using PV and BESS connected directly to DC-link. The DFIG contains two converters, RSC and GSC linked back-to-back through a DC-link. MFO-FLC has been implemented for optimizing the scaling factors of FLC for GRC and RSC controllers. PV array MPPT is implemented using the MFO-FLC technique and an optimized constant-current constant-voltage MFO-PI controller is designed to control the charging and discharging of BESS.

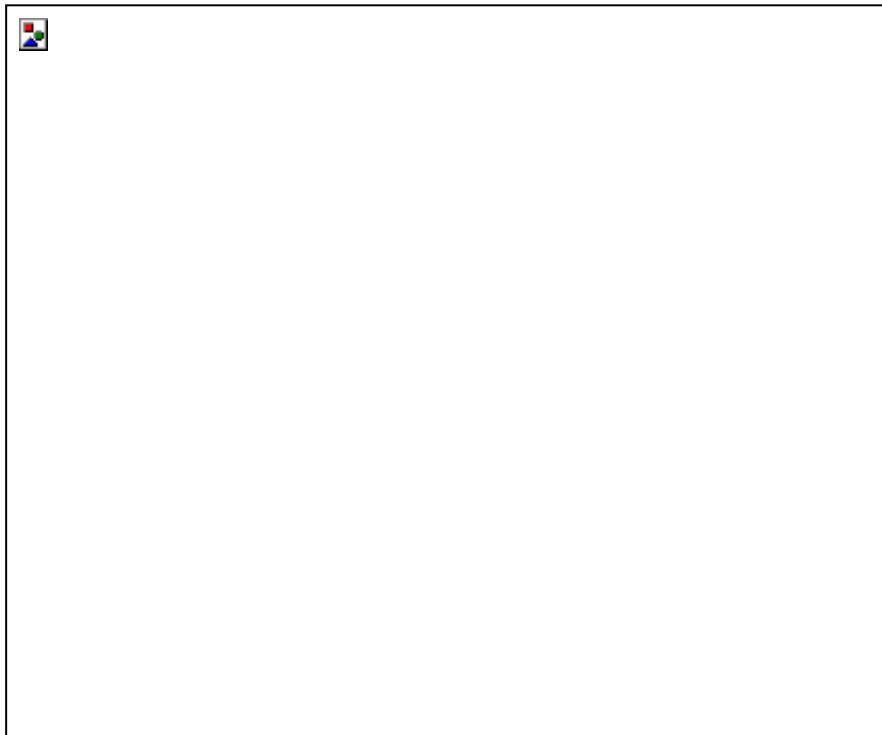


**Fig. 1.** Configuration of hybrid PV-BESS for grid-connected DFIG based WECS.

Figure 2 shows the flowchart of the proposed control and power management strategy. Based on variable wind speed and solar radiation conditions, PV-BESS has been implemented to adjust the  $V_{dc}$ , minimize the rotor current's peak value, and maintain active power stabilization under

wind speed variation. MFO has been chosen as the optimization technique to obtain the optimized parameters of different proposed controllers. As a result, the system's performance will improve, and the best controller step response results will be obtained. The control of the DFIG

wind turbine is carried out using fuzzy logic controllers, which control the dc-Link voltage and current controllers of the grid-side and rotor-side converters. The scaling factors of these controllers are optimized using MFO. The PV system is connected to the DC-link via a boost DC-DC converter. Hence, the main controller of the PV system is the MPPT controller. The output from this controller is the duty cycle that drives the switch of the boost DC-DC converter. In this paper, an optimized MFO-FLC is proposed for the MPPT controller of the PV array. While the battery management control is implemented through an optimized constant-current constant-voltage MFO-PI controller. The energy management strategy and control of the hybrid wind PV-BESS system shown in the flowchart can be summarized as follows:

- Because the PV-BESS is the most important component at this point, the power management control inquiries about its battery state of charge (SOC) and PV

output power. If  $SOC = SOC_{max}$  (100%) and the wind speed is at the rated speed, then, the battery current and power are both set to 0 at this point, The PV is disconnected, and the total power provided to the grid is the output of DFIG ( $P_w$ ).

- If the rotational speed of DFIG is below the rated speed (super-synchronous mode), the control asks if the  $SOC_{min} < SOC \leq SOC_{max}$ , then the battery begins to discharge. PV and battery power are then delivered to the grid to compensate for the power loss and keep the DC-link voltage constant during wind transitions.

- At high wind speeds above the rated (sub-synchronous mode), the controller checks if the  $SOC < SOC_{max}$ , and the PV power equal to zero, then the battery will begin to charge, and a portion of the power is absorbed from the grid. If the PV power is higher than zero, the battery will charge from the DFIG wind turbine and PV array. The DC-link voltage is kept constant in all modes of operation



Fig. 2. Optimal control and energy management flow chart.

2.1 Wind Turbine Model

Wind turbines are prime movers that convert kinetic wind energy into mechanical rotational energy. The wind speed  $v$  and power capture coefficient  $C_p$  were utilized to calculate

the mechanical power converted. The mechanical power  $P_m$  captured by a three-blade horizontal axis wind turbine is often expressed using the following expression [28]:

$$P_m = \frac{1}{2} \rho A v^3 C_p \tag{1}$$

Here,  $\rho$  is the air density ( $\text{kg/m}^3$ ), and  $C_p$  the coefficient of the wind turbine is based on  $\lambda$  as well as  $r$  is the radius of the blades (m). The ratio of the blade speed to the wind speed is  $\lambda$ :

$$\lambda = \frac{v_{tip}}{v_{wind}} \quad (2)$$

$$C_p = \frac{16}{21} \lambda^3 \left( 1 - \frac{1}{\lambda} \right) \quad (3)$$

**2.2 Photovoltaic Array Model**

Many configurations of PV modules are used in the literature, but the single diode equivalent circuit is shown in Figure 3 is the most widely utilized, and the PV cell is modeled by the following main function, which describes the current and the voltage characteristics [31-34].

$$I = I_L - I_{sat} \left[ \exp \left( \frac{V + I R_s}{n V_t} \right) - 1 \right] - \frac{V + I R_s}{R_p} \quad (4)$$

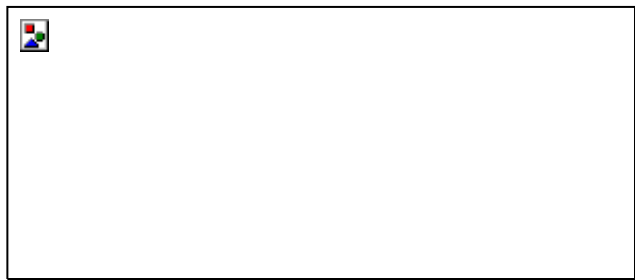


**Fig. 3.** PV cell equivalent circuit.

Where,  $I_L$ ,  $I_{sat}$ , and  $I_{sc}$  are the photocurrent, the solar panel's reverse saturation current, and short circuit current respectively.  $N_s$  is the number of cells in series and  $m$  is the diode's ideal factor.  $K$  is the Boltzmann constant ( $1.381 \times 10^{-23} \text{ J/K}$ ) and  $q$  is the electron's charge ( $1.6021 \times 10^{-19} \text{ C}$ ).  $R_s$  and  $R_p$  are the series and parallel resistances, respectively.  $G$  and  $G_{ref}$  denote the actual and nominal amounts of irradiation, respectively. The temperature degree in kelvin (K) is denoted by  $T$ , while the current temperature coefficient is denoted by  $\alpha_i$ .  $V_{oc}$  is an open-circuit voltage at standard test conditions.

**2.2.1 PV Sizing**

The specifications of the PV module (Topsun TS-M400JA1) that used in this design are ( $P_{max}$ ) is 400.0724 KW, ( $V_{oc}$ ) is 61.1 V, ( $I_{sc}$ ) is 8.62A, according to a maximum power point voltage ( $V_{MPP}$ ) and current ( $I_{MPP}$ ) are 49.27 V and 8.12 A, respectively. To implement the proposed PV system, the required number of modules can be calculated using the following equation [35]:

$$N_{pv} = \frac{P_{req}}{P_{max}} \quad (5)$$

$$N_{pv} = \frac{P_{req}}{P_{max}} \quad (5)$$

Where required power is equal to 25% of the total power given by DFIG, as explained in [36], and the required number of series-connected photovoltaic modules ( $N_{pv,s}$ ) is calculated as

$$N_{pv,s} = \frac{V_{dc}}{V_{MPP}} \quad (6)$$

$$N_{pv,p} = \frac{P_{req}}{N_{pv,s} P_{max}} \quad (7)$$

The photovoltaic array's strings can be calculated using the following equation:

$$N_{strings} = \frac{N_{pv}}{N_{pv,p}} \quad (8)$$

As a result, the PV system is designed to be 12 series modules and 79 parallel strings, as can be cleared in Figure 4.

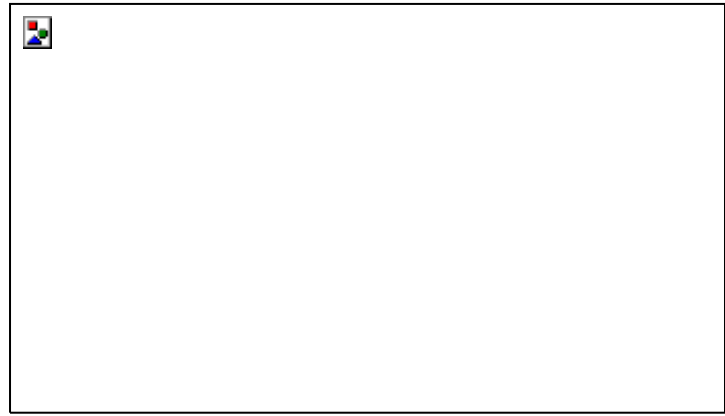


**Fig. 4.** Configuration of PV array

**2.2.2 PV MPPT**

Figure 5 clarifies the PV characteristics, the maximum power will only occur at the  $P_{max}$ . An intelligence [32] MFO-FLC technique is used to adjust the duty cycle of a DC-DC converter. That guarantees the occurrence of maximizing the output of the PV modules instead of the P&O method, so we ensure that the solar panel's maximum output power is extracted regardless of operational conditions.

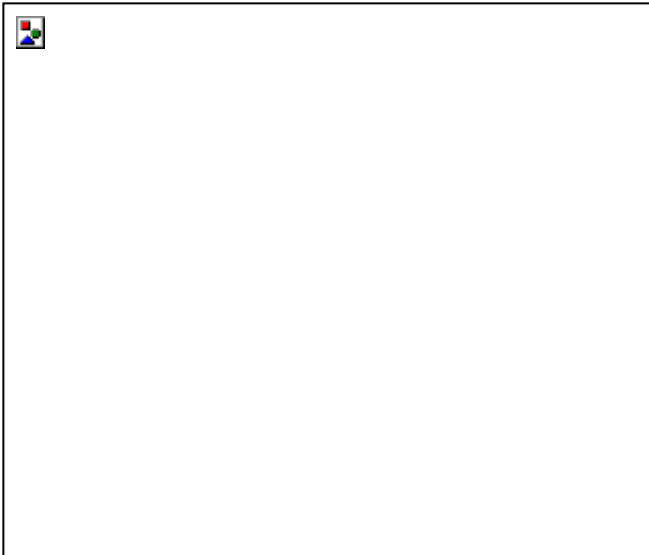


**Fig. 5.** I-V and P-V characteristics for PV array at variable solar radiation.

Three functional blocks define the FLC used in MPPT: fuzzification, fuzzy rule basis, and defuzzification. The error  $E(t)$  and  $dE(t)$  are input signals to FLC. Two inputs are converted into the FLC's output by input gain factors ( $1/K_e$ ,  $1/K_{de}$ ), and ( $1/K_u$ ) as output gain. MPPT is based on the incremental conductance algorithm as cleared in equation 8. The block diagram of FLC is depicted in Figure 6. The most frequently encountered FLC application is the triangle membership function. Straight lines are used to create the triangular MF. MFS's straight lines have an advantage in terms of simplicity. Negative Big (NB), Negative Medium (NM), Negative Small (NS), Zero (ZE), Positive Small (PS), Positive Medium (PM), and Positive Big (PB) are the seven triangle memberships utilized for the inputs and outputs (PB) as clear in Figure 7. As shown in Appendix 1, 49 rules are obtained from the  $7 \times 7$  matrix. Figure 8 illustrates the fuzzy controller's optimum surface area curve (The FLC surface at MFO optimized scaling factors). The error (E), the optimization algorithm's objective function, is calculated from the incremental conductance algorithm as shown in equation 8 [37] [38].



**Fig. 6.** MPPT based FLC.

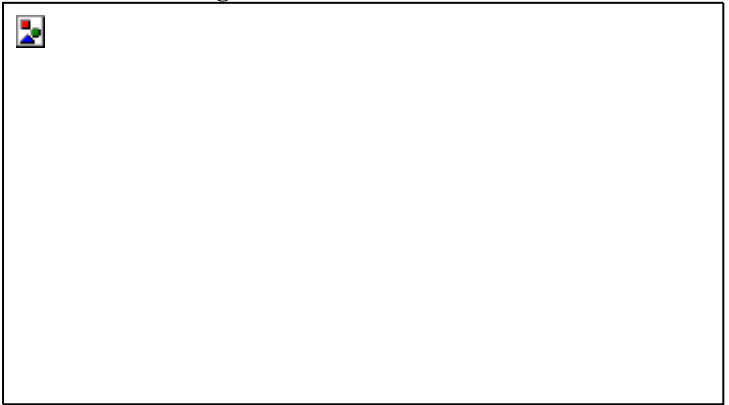


**Fig. 7.** MF of Fuzzy controller.

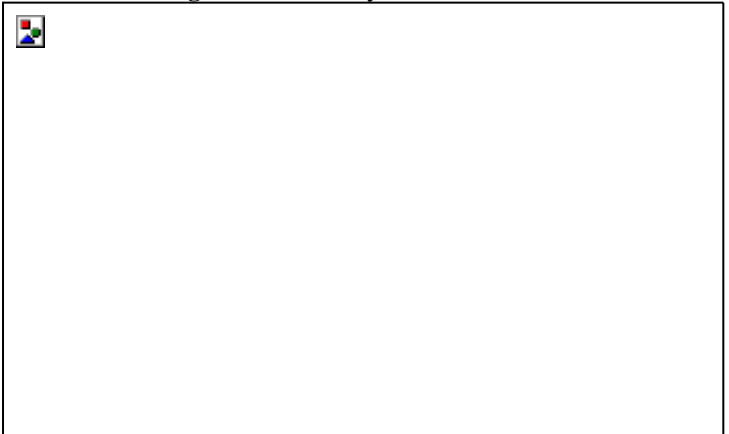


**Fig. 8.** Fuzzy controller's surface.

(8)

The following sections discuss MFO optimization strategies for FLC [39]. To begin MFO, moths are released into the search area at random. After that, it uses a flame to determine the optimal position for each moth. Finally, the moths' positions are adjusted using a spiral movement function so that they can land in the ideal positions indicated by a flame:

(9)

(10)

(11)

Here,  $\left[ \begin{matrix} \text{moth} \\ \text{flame} \end{matrix} \right]$  represents the  $i$ th moth and the  $j$ th flame,  $\left[ \begin{matrix} \text{moth} \\ \text{flame} \end{matrix} \right]$  denotes the logarithmic maturation pattern model's variability,  $z$  denotes a random value between  $[-1, 1]$ , and  $D_i$  means the distance between the  $i$ th moth and the  $j$ th flame. Then, using the following formula, update the flame number:

$$\left[ \begin{matrix} \text{moth} \\ \text{flame} \end{matrix} \right] = \left[ \begin{matrix} \text{moth} \\ \text{flame} \end{matrix} \right] + z \cdot D_i \quad (12)$$

Where  $N$  denotes the total number of flames,  $l$  denotes the current iteration, and  $T$  denotes the total number of iterations. Continue this process until reached the stopping point, and then add the new best moths to the optimizer.

### 2.3 Battery Energy Storage System Model

Solar and wind energy systems use lead-acid batteries, they have a high power-to-weight ratio and are cost-effective. For lead-acid batteries, there are a lot of different types in the global market. Thevenin equivalent circuit model [40] described components of the battery model. It has a no-load voltage ( $V_o$ ), internal resistance ( $R_1$ ), a capacitor ( $C$ ), and  $R_2$  is the resistance of the plate. In appendix 2, we describe the parameters of BESS according to system needs. Ref [40] includes the battery model illustrated in Figure 9, which is not an optimized battery design. SOC is described in [41] based on the percentage of battery reserve capacity (actual battery capacity divided by rated battery capacity). Accordingly, when we choose an optimum battery size (which is required owing to system requirements), we must investigate the state of charge of the battery and build a control strategy based on that. In this proposed system, the constant-current/ constant-voltage controller is implemented on the batteries using MFO-PI as shown in Figure 10. An optimized PI controller on the batteries is designed by using the MFO technique which was explained in detail in the previous section. As a result of using these MFO-PI controllers, the system's major characteristic will be optimal performance, which makes it more stable and gives the best results, through which system performance improves occurs in the system and maintain the constant power and  $V_{dc}$ , under the conditions of variable solar radiation wind speed.

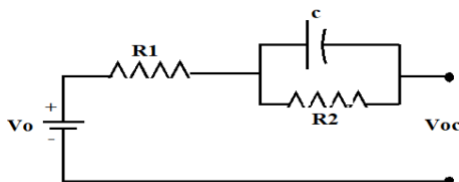


Fig. 9. Lead-acid BESS model

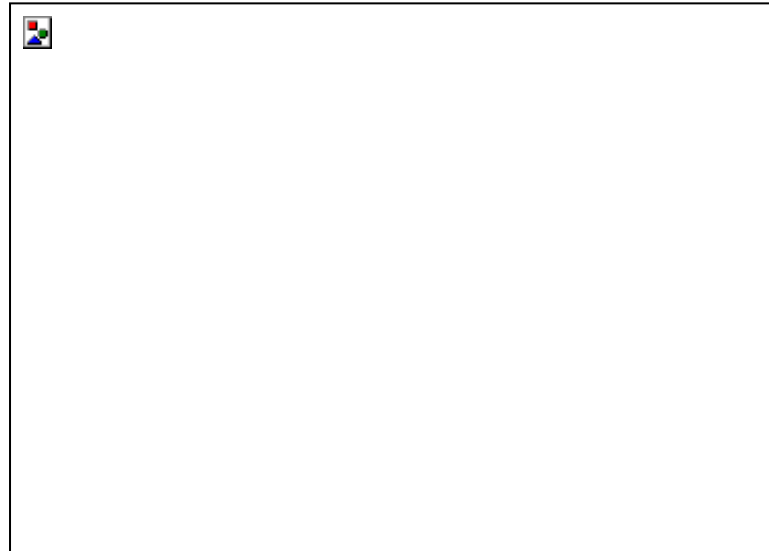


Fig. 10. CC-CV BESS controller.

When sizing a battery system, the most essential step is to calculate the required or desired amount of energy storage [42] [43], which is usually expressed in kWh per day, the following equation is used:

$$\left[ \begin{matrix} \text{moth} \\ \text{flame} \end{matrix} \right] = \left[ \begin{matrix} \text{moth} \\ \text{flame} \end{matrix} \right] + z \cdot D_i \quad (13)$$

Where,  $I_d$  is the discharging current (A) and  $T_d$  is the discharging time (h). The battery must store energy for several days and be used without exceeding the maximum DOD. The following formula can be used:

$$\left[ \begin{matrix} \text{moth} \\ \text{flame} \end{matrix} \right] = \left[ \begin{matrix} \text{moth} \\ \text{flame} \end{matrix} \right] + z \cdot D_i \quad (14)$$

$Q$  denotes the needed minimum battery capacity (Ah),  $E$  energy needs within the day (Wh),  $A$  is the number of days is needed for battery storage,  $V$  system DC voltage (V), DOC is the battery depth of discharge, which is normally listed on the datasheet (typically 0.3-0.9),  $\eta_{inv}$  is converter efficiency and  $\eta_{cable}$  Electricity cable efficiency refers to the efficiency of the cables that transport electricity from the battery to the loads. In this paper, the rated battery capacity is calculated based on the rated power of the DFIG wind turbine, the overall power of PV and BESS transferred via the back-to-back converter to the grid does not exceed 25% of the wind turbine power rating (See Appendix 2 for the calculated battery size).

### 2.4 Design And Control Of Hybrid Wind PV-BESS System

Figure 11 depicts a schematic diagram of the DFIG based WECS with the proposed control. The proposed scheme consists of a hybrid PV-BESS system into the DC-link of the DFIG back-to-back converter. The proposed system is controlled by MFO-FLC. Equation 16 shows how the error

$E(t)$  is calculated by comparing a reference value ( $V_{dref}$ ) to the dc-link voltage ( $V_{dc}$ ) of the back-to-back converter. The new DC-link voltage for the hybrid PV-BESS wind system can be calculated from the current balance provided by equation 17 [44-46].



(15)



(16)

Where  $I_{dg}$ ,  $I_{dr}$ ,  $I_{PV}$ , and  $I_b$  are the d-component of grid current, d-component of rotor current, PV, and battery currents, respectively.



**Fig. 10.** Block diagram of the proposed system.

**3. Results and Discussion**

MATLAB Sim-power-system is used to design and simulate a model for the proposed system consisting of hybrid PV-BESS for grid-connected 1.5 MW DFIG based WECS. The appendices (2, 3 and 4) contain a list of the simulation parameters. The stator is linked directly to the grid, whereas the terminals of the rotor are connected via a back-to-back converter, and the PV array and BESS are connected directly into a DC-link. Variation in wind speed below and above the rated speed is regarded. Also,

the change in solar radiation has been considered at a constant ambient temperature (25°C). The Simulation results present a comparison between the proposed optimized system with PV and BESS and the PI-based controller without PV and BESS. The proposed system's management strategy can be explained as follows:

MFO-FLC is used to implement optimal control of the DFIG; DC-link voltage control, and current regulators for GSC and RSC converters.

Another MFO-FLC is used to develop an optimal MPPT technique, which is then tested under variable solar radiation and a constant photovoltaic temperature of 25°C.

Step changes in wind speed are taken into account while running the simulation. Wind speed variations below and above the rated speed are considered, as shown in Figure 12. The wind speed is maintained at 16 m/s for the first 10 seconds. Then the speed of wind is varied to 8 m/s until 20 seconds.

The simulation results will be discussed as follows:

Figure 12 shows the input wind speed pattern and the DC-link voltage. When the proposed system based on the MFO-FLC controller is compared to the system without PV-BESS, it is clear that the MFO-FLC controller performs optimally in terms of transient response, less overshoot, faster settling time, and tries to keep the constant voltage on the DC-link as stable as possible during steady-state.

Figure 13 represents the DFIG wind power without and with PV-BESS system under variable wind speed and different radiation levels. The wind speed varies in each run, but the solar radiation remains constant at a predetermined level. As shown in Figure 13, the active power injected by DFIG at 16 m/s wind speed (from 0 to 10 seconds) is 1.5 MW (rated) at all solar radiation values. The transient response is better, and the active power output is smoothed at transient and steady-state conditions when solar radiation is high. Overall the hybrid PV-BESS wind system gives a better response than the wind system alone, and the active power is boosted and smoothed.

Whereas a change in wind speed from high to low caused the active power to temporarily fall below the expected value, the real power delivered to the grid then becomes the active power generated by the DFIG, plus the power of the battery discharge and reached 0.83 MW at 1000 W/m<sup>2</sup> solar radiation. The percentage increase in the power is 22% than the case of wind turbine only.

Figure 14 depicts SOC behaviour under changeable solar radiation and variable wind speed, the figure illustrated that battery charging (from 0 to 10 sec) when wind speed is 16 m/s. The state of charge (SOC) increases as the solar radiation increases to 90.055% SOC at 1000 W/m<sup>2</sup> solar radiation. When wind speed decreased (at t = 10 sec) we noted that the battery discharged at (0, 250, and 500 W/m<sup>2</sup> solar radiation, respectively). In this case, the PV-BESS system participates in increased active power injected by DFIG 22 % at 1000 W/m<sup>2</sup>.

Another case study is discussed using variable solar radiation at different wind speeds (the wind speed is kept constant for each run). Figure 15 represents solar radiation pattern, PV voltage, PV output power, and PV plus battery power delivered to the grid. The solar radiation is presented by a step change starting from 250 W/m<sup>2</sup> and changes every 2 seconds to increase by a step change to 500 and 1000 W/m<sup>2</sup>, respectively, the decrease at the same rate. Figure 15 depicts that MPPT based on the MFO-FLC gives the best performance, the PV voltage is kept at the maximum value as it is important to keep it constant at 591.5 V converted to 1150 V via the boost DC-DC converter (0.4859 optimal duty cycle output from MFO-FLC). PV gives the maximum power based on the proposed control at different solar radiation values, as shown in Figure 15. The total PV and battery power delivered to or absorbed from the grid are also shown in this figure. It is clear that the batteries are charging at wind speeds higher or equal rated speed and when wind speed is less than rated batteries begins discharging and participating in the active energy delivered to the grid, accordingly, better performance and stability of the system are maintained with random changes in wind speeds.

#### 4. Conclusion

An optimized control strategy for a grid-connected DFIG based WECS system using PV and BESS was implemented to maintain a constant DC-link voltage, boost and smooth the active power delivered to the grid under variation in wind speed and solar radiation. The optimized proposed control includes intelligent MFO-FLC control of the DFIG's stator and rotor currents, as well as the use of MFO-FLC for MPPT for PV and optimal control MFO-PI for battery charging/discharging control. The system is implemented and tested in the MATLAB Simulink environment.

Simulation results showed that the improved intelligent control techniques give a very excellent behavior; stabilizing active power as much as possible and smoothing the fluctuation of the DC-link voltage under variable wind speed and solar radiation. Furthermore, when the PV-BESS system is integrated into the DC-link of the DFIG's back-to-back converter, the active power delivered to the grid is increased by 22%.

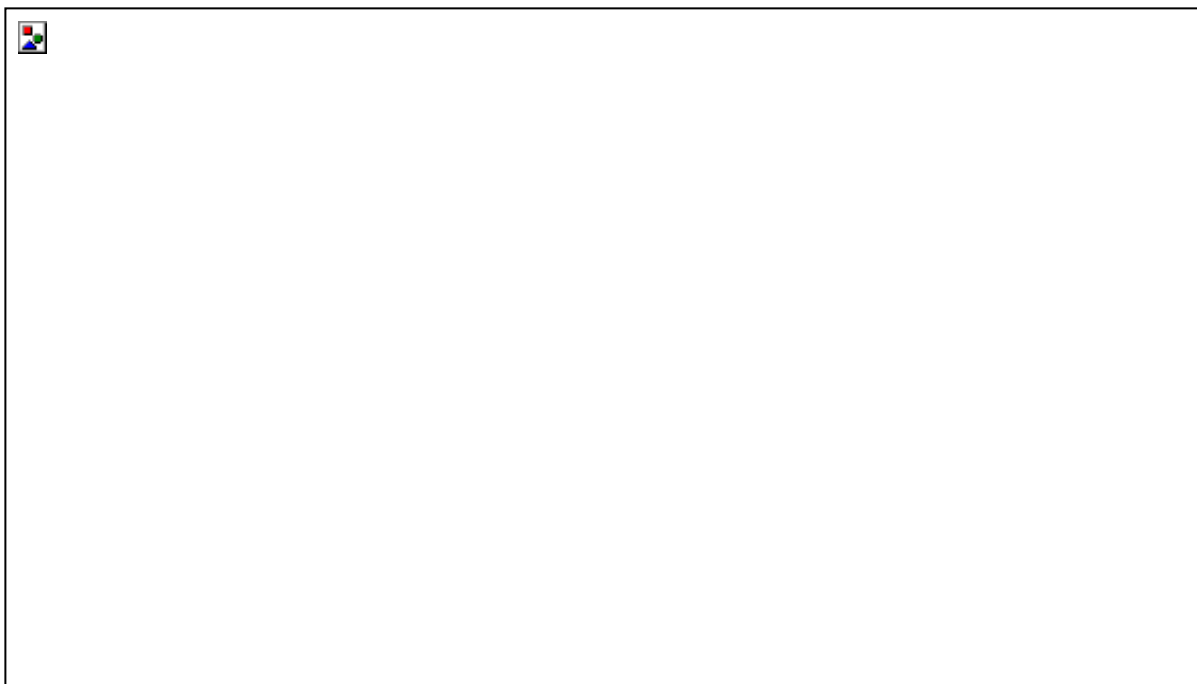


**Fig. 12.** DC-link voltage under wind variation.

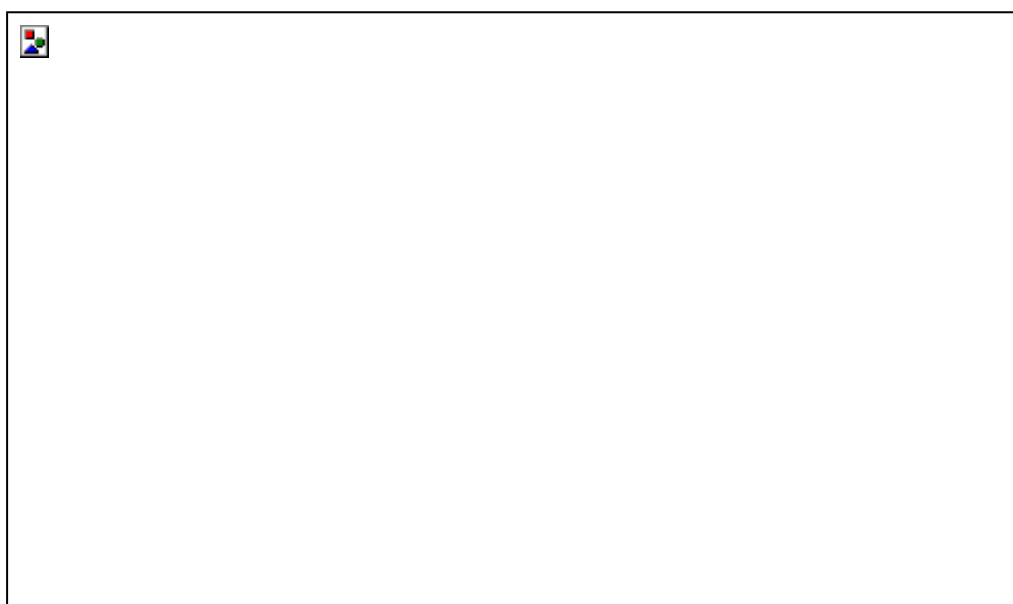


**Fig. 13.** Active power delivered to the grid.

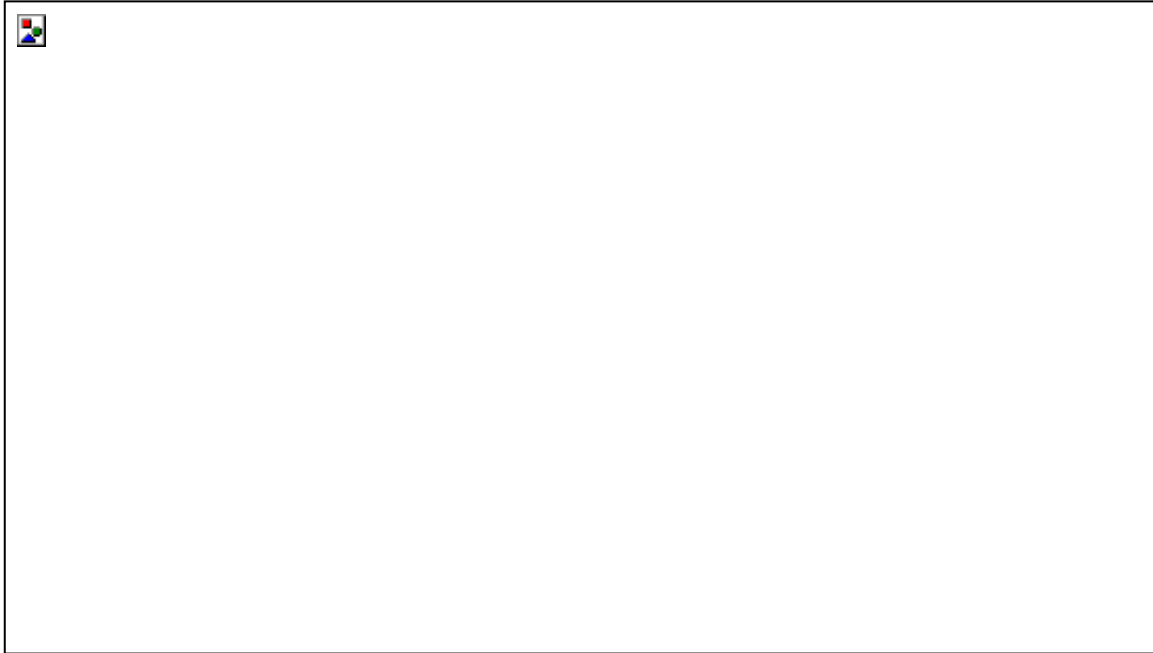


**Fig. 14.** SOC behavior for variable solar radiation.



**Fig. 15.** PV voltage and power under variable solar radiation and wind speed.

## References

- [1] S. Saib and A. Gherbi, "Simulation and control of hybrid renewable energy system connected to the grid", 5th International Youth Conference on Energy, DOI: 10.1109/IYCE.2015.7180818, Aug. 2015.
- [2] X. Kong, X. Liu, L. Ma, and K. Y. Lee, "Hierarchical Distributed Model Predictive Control of Standalone Wind/Solar/Battery Power System", *IEEE Trans. Syst. Man, Cybern. Syst.*, DOI: 10.1109/TSMC.2019.2897646, vol. 49, No. 8, pp. 1570–1581, Aug. 2019.
- [3] K. D. Mercado, J. Jiménez and M. C. G. Quintero, "Hybrid renewable energy system based on intelligent optimization techniques", 2016 IEEE International Conference on Renewable Energy Research and Applications (ICRERA), pp. 661-666, DOI: 10.1109/ICRERA.2016.7884417, 2016.
- [4] O. P. Mahela, B. Khan, H. H. Alhelou, and P. Siano, "Power Quality Assessment and Event Detection in Distribution Network with Wind Energy Penetration Using Stockwell Transform and Fuzzy Clustering", *IEEE Trans. Ind. Informatics*, DOI: 10.1109/TII.2020.2971709, vol. 16, No. 11, pp. 6922–6932, Nov. 2020.
- [5] U. Akram, M. Khalid, and S. Shafiq, "An innovative hybrid wind-solar and battery-supercapacitor microgrid system—development and optimization", DOI: 10.1109/ACCESS.2017.2767618, vol. 5, pp. 25897–25912, Oct. 2017.
- [6] S. Vadi, F. B. Gürbüz, R. Bayindir and E. Hossain, "Design and Simulation of a Grid Connected Wind Turbine with Permanent Magnet Synchronous Generator", 2020 8th International Conference on Smart Grid (icSmartGrid), pp. 169-175, DOI: 10.1109/icSmartGrid49881.2020.9144762, 2020.
- [7] Y. Charabi and S. Abdul-Wahab, "Wind turbine performance analysis for energy cost minimization", *Renewables*, DOI: 10.1186/s40807-020-00062-7, vol. 7, No. 5, 2020.
- [8] M. A. Soliman, H. M. Hasanien, A. Al-Durra, and I. Alsaidan, "A novel adaptive control method for performance enhancement of grid-connected variable-speed wind generators", *IEEE Access*, DOI: 10.1109/ACCESS.2020.2991689, vol. 8, pp. 82617–82629, 2020.
- [9] M. Quraan, Q. Farhat, and M. Bornat, "A new control scheme of back-to-back converter for wind energy technology", 6th Int. Conf. Renew. Energy Res, pp. 354–358, Appl. ICRERA, 2017.
- [10] M. H. Qais, H. M. Hasanien, and S. Alghuwainem, "A novel LMSRE-based adaptive PI control scheme for grid-integrated PMSG-based variable-speed wind turbine", *Int. J. Electr. Power Energy Syst.*, DOI: 10.1016/j.ijepes.2020.106505, vol. 125, p. 106505, August 2020.
- [11] M. Qais, H. M. Hasanien, and S. Alghuwainem, "Salp swarm algorithm-based TS-FLCs for MPPT and fault ride-through capability enhancement of wind generators", *ISA Trans.*, DOI: 10.1016/j.isatra.2020.01.018, vol. 101, pp. 211–224, 2020.
- [12] F. Mazouz, S. Belkacem, I. Colak, "DPC- SVM of DFIG Using Fuzzy Second Order Sliding Mode Approach", *Int. J. Smart grid*, DOI: 10.20508/ijsmartgrid.v5i4.219.g178, vol. 5, No. 4, 2021.
- [13] L. Amira, B. Tahar, and M. Abdelkrim, "Sliding Mode Control of Doubly-fed Induction Generator in Wind Energy Conversion System", 8th Int. Conf. Smart Grid, pp. 96–100, icSmartGrid, 2020.
- [14] S. K. Tiwari, B. Singh, and P. K. Goel, "Design and control of autonomous wind-solar energy system with DFIG feeding 3-phase 4-wire network", 12th IEEE Int. Conf. Electron. Energy, Environ. Commun. Comput. Control E3-C3, DOI: 10.1109/INDICON.2015.7443822, 2016.
- [15] A. Hamadi, S. Rahmani, K. Addoweesh, and K. Al-Haddad, "A modeling and control of DFIG wind and PV solar energy source generation feeding four-wire isolated load", *IECON Proc. Industrial Electron. Conf.*, pp. 7778–7783, 2013.
- [16] S. K. Tiwari, B. Singh, and P. K. Goel, "Design and Control of Autonomous Wind-Solar System with DFIG Feeding 3-Phase 4-Wire Loads", *IEEE Trans. Ind. Appl.*, DOI: 10.1109/TIA.2017.2780168, vol. 54, No. 2, pp. 1119–1127, 2018.
- [17] A. Kumar, Shivashankar, and Keshavamurthy, "Design and control of autonomous hybrid wind-solar system with DFIG supplying three-phase four-wire loads", *Ain Shams Eng. J.*, DOI: 10.1016/j.asej.2020.11.027, 2021.
- [18] T. Mesbahi, A. Ouari, T. Ghennam, E. Berkouk, N. Rizoug, N. Mesbahi, M. Meradji, "A stand-alone wind power supply with a Li-ion battery energy storage system", *Renew. Sustain. Energy Rev.*, DOI: 10.1016/j.rser.2014.07.180, vol. 40, pp. 204–213, 2014.
- [19] N. Mendis, K. M. Muttaqi, and S. Perera, "Active power management of a super capacitor-battery hybrid energy storage system for standalone operation of DFIG based wind turbines", *Conf. Rec. - IAS Annu. Meet. IEEE Ind. Appl. Soc.*, DOI: 10.1109/IAS.2012.6374045, pp. 1–8, 2012.
- [20] N. Mendis, K. M. Muttaqi, and S. Perera, "Management of low- and high-frequency power components in demand-generation fluctuations of a DFIG-based wind-dominated RAPS system using hybrid energy storage", *IEEE Trans. Ind. Appl.*, DOI: 10.1109/TIA.2013.2289973, vol. 50, No. 3, pp. 2258–2268, 2014.
- [21] L. Miao, J. Wen, H. Xie, C. Yue, and W. J. Lee, "Coordinated Control Strategy of Wind Turbine Generator and Energy Storage Equipment for Frequency

- Support”, IEEE Trans. Ind. Appl., DOI: 10.1109/TIA.2015.2394435, vol. 51, No. 4, pp. 2732–2742, 2015.
- [22] V. Knap, R. Sinha, M. Swierczynski, D. I. Stroe, and S. Chaudhary, “Grid inertial response with Lithium-ion battery energy storage systems”, IEEE Int. Symp. Ind. Electron, DOI: 10.1109/ISIE.2014.6864891, pp. 1817–1822, 2014.
- [23] B. Peng, F. Zhang, J. Liang, L. Ding, Z. Liang, and Q. Wu, “Coordinated control strategy for the short-term frequency response of a DFIG-ES system based on wind speed zone classification and fuzzy logic control”, Int. J. Electr. Power Energy Syst., DOI: 10.1016/j.ijepes.2018.11.010, vol. 107, No. June 2018, pp. 363–378, 2019.
- [24] N. K. S. Naidu and B. Singh, “Grid-Interfaced DFIG-Based Variable Speed Wind Energy Conversion System with Power Smoothing”, IEEE Trans. Sustain. Energy, DOI: 10.1109/TSTE.2016.2582520, vol. 8, No. 1, pp. 51–58, 2017.
- [25] L. A. G. Gomez, A. P. Grilo, M. B. C. Salles, and A. J. S. Filho, “Combined control of DFIG-based wind turbine and battery energy storage system for frequency response in microgrids”, Energies, DOI: 10.3390/en13040894, vol. 13, No. 4, 2020.
- [26] S. A. Abo-alela, “Design and Performance of Hybrid Wind-Solar Energy”, J. AL AZHAR Univ. Eng. Sect, vol. 13, No. 48, pp. 1118–1124, July 2018.
- [27] S. Puchalapalli and B. Singh, “A Grid Interactive Microgrid Based on Wind Driven DFIG and Solar PV Array with Regulated Power Flow Functionality”, *8th IEEE India International Conference on Power Electronics (IICPE)*, pp. 1-6, 2018.
- [28] P. K. Anju and P. P. Zarina, “Power Fluctuation Reduction Using Battery System in DFIG Based Wind Energy Conversion System”, Proc. 2018 Int. Conf. Curr. Trends Towar. Converging Technol, pp. 1–5, ICCTCT 2018.
- [29] P. Gajewski, K. Pienkowski, “Control of the Hybrid Renewable Energy System with Wind Turbine, Photovoltaic Panels and Battery Energy Storage”, Energies, DOI: 10.33390/en14061595, vol.14, 2021.
- [30] A. Bouraiou, M. Hamouda, A. Chaker, M. Sadok, M. Mostefaoui, and S. Lachtar, “Modeling and Simulation of Photovoltaic Module and Array Based on One and Two Diode Model Using Matlab/Simulink”, Energy Procedia, DOI: 10.1016/j.egypro.2015.07.822, vol. 74, pp. 864–877, 2015.
- [31] H. Bakir and A. A. Kulaksiz, “Modelling and voltage control of the solar-wind hybrid micro-grid with optimized STATCOM using GA and BFA”, Eng. Sci. Technol. an Int. J., DOI: 10.1016/j.jestch.2019.07.009, No. August, 2019.
- [32] X. Ge, F. W. Ahmed, A. Rezvani, N. Aljojo, S. Samad, and L. K. Foong, “Implementation of a novel hybrid BAT-Fuzzy controller based MPPT for grid-connected PV-battery system, Control Eng. Pract., DOI: 10.1016/j.conengprac.2020.104380, vol. 98, Article. 104380, 2020.
- [33] V. Viswanatha, R. Venkata Siva Reddy, “Microcontroller based bidirectional buck-boost converter for photo-voltaic power plant”, J. Electr. Syst. Inf. Technol., DOI: 10.1016/j.jesit.2017.04.002, vol. 5, No. 3, pp. 745–758, 2018.
- [34] K. Venkatesan and U. Govindarajan, “Optimal power flow control of hybrid renewable energy system with energy storage: A WOANN strategy”, J. Renew. Sustain. Energy, DOI: 10.1063/1.5048446, vol. 11, No. 1, 2019.
- [35] A. Q. Al-shetwi and M. Z. Sujod, “Sizing and Design of PV Array for Photovoltaic Power Plant Connected Grid Inverter, Natl. Conf. Postgrad., Univ. Malaysia Pahang, pp. 193–199, 2016.
- [36] R. Al Badwawi, M. Abusara, T. Mallick, “A review of hybrid solar PV and wind energy system”, Smart Science, DOI: 10.6493/SmartSci.2015.324, vol. 3, pp. 127-138, April 2015.
- [37] M. Kumar, S. R. Kapoor, R. Nagar, and A. Verma, “Comparison between IC and Fuzzy Logic MPPT Algorithm Based Solar PV System using Boost Converter”, International Journal of Advanced Research in Electrical, Electronics and Instrumentation Engineering, DOI: 10.15662/ijareeie.2015.0406007, vol. 4, Issue 6, pp. 4927–4939, 2015.
- [38] N. M. Yasin and H. M. Abd Alhussain, “Improved Efficiency of photovoltaic Module Based on Fuzzy Logic MPPT Technique”, IOP Conf. Ser. Mater. Sci. Eng, DOI: 10.1088/1757-899X/745/1/012006, vol. 745, no. 1, 2020.
- [39] S. Mirjalili, “Moth-Flame Optimization Algorithm: A Novel Nature-inspired Heuristic Paradigm”, KNOWLEDGE-BASED Syst., DOI: 10.1016/j.knosys.2015.07.006, July, 2015.
- [40] J. J. Kelly and P. G. Leahy, “Optimal investment timing and sizing for battery energy storage systems”, journal of Energy Storage, DOI: 10.1016/j.est.2020.101272, vol. 28, 2020.
- [41] J. Boyle, T. Littler, and A. Foley, “Battery energy storage system state-of-charge management to ensure availability of frequency regulating services from wind farms”, Renew. Energy, DOI: 10.1016/j.renene.2020.06.025, vol. 160, pp. 1119–1135, 2020.
- [42] M. Shabani, E. Dahlquist, F. Wallin, and J. Yan, “Techno-economic impacts of battery performance models and control strategies on optimal design of a grid-connected PV system, Energy Convers. Manag., DOI: 10.1016/j.enconman.2021.114617, vol. 245, Article. 114617, 2021.
- [43] Z. M. Salameh, M. A. Casacca, and W. A. Lynch, “A mathematical model for lead-acid batteries”, IEEE

Trans. Energy Convers., DOI: 10.1109/60.124547, vol. 7, No. 1, pp. 93–98, 1992.

[44] M. Shehab, L. Abualigah, H. Al Hamad, H. Alabool, M. Alshinwan, and A. M. Khasawneh, “Moth-flame optimization algorithm: variants and applications”, Neural Computing and Applications, DOI: 10.1007/s00521-019-04570-6, vol. 32, No. 14. Springer, pp. 9859–9884, Jul. 2020.

[45] C. R. Algarín, J. T. Giraldo, and O. R. Álvarez, “Fuzzy logic based MPPT controller for a PV system, Energies, DOI: 10.3390/en10122036, vol. 10, No. 12, 2017.

[46] T. Riouch, R. El-Bachtiri, A. Alamery, and C. Nichita, “Control of battery energy storage system for wind turbine based on DFIG during symmetrical grid fault”, Renew. Energy Power Qual. J., DOI: 10.24084/repqj13.465, vol. 1, No. 13, pp. 714–718, 2015.

Appendix 1: FLC rules

E(t)	ΔE(t)						
	NB	NM	NS	ZE	PS	PM	PB
NB	NB	NB	NB	NB	NM	NS	ZE
NM	NM	NM	NS	NS	NM	ZE	PS
NS	NB	NB	NM	NS	ZE	PS	PM
ZE	NB	NM	NS	ZE	PS	PM	PB
PS	NM	NS	ZE	PB	PM	PB	PB
PM	NS	ZE	PS	PM	PB	PB	PB
PB	ZE	PS	PM	PB	PB	PB	PB

Appendix 2: BESS parameters

Parameter	Value
Bi-directional DC-D Converter inductance (H)	0.5e-3
capacitance (F)	1200e-6
Rated battery capacity (AH)	6500
DOD	90%
Nominal Battery Voltage (V)	575

Appendix 3: DFIG wind turbine parameters

DFIG		
Vbase = 575 V Rs = 0.023 p.u. Ls = 3.08 p.u. Hgenerator = 0.685 s	P= 1.5 MW Rr = 0.016 p.u. Lr = 3.06 p.u. Nr /Ns = 3.43	Fbase = 50 Hz Ωbase = 2π*Fbase = 314 rad/s Lm = 2.9 p.u. No. P = 3
GSC		
Vdcrated = 1150 V Cdc = 10 Mf	Rg = 0.003 p.u. Rfilter = 50 mΩ	Lg = 0.3 p.u. Cfilter = 1 Mf
Mass drive train		

K Shaft spring constant = 1.11 p.u.	D Shaft mutual damping = 1.5 p.u.
WT	
Ratio pf gearbox = 65.5 m H height = 65 m ωturbine-base = 1.92 rad/s R1 = 0.1153 Ω/km R0 = 0.413 Ω/km	

Appendix 4: PV array DC-DC boost converter parameters

Parameter	Value
Duty ratio	0.48591
Switching frequency (kHz)	5
Input boost DC-DC converter inductance (H)	0.4791e-4
PV input DC-link capacitance (F)	1200e-6
Output boost DC-DC converter capacitance (F)	5.5729e-4